

Titania Nanotube-Stabilized BiOCl Nanoparticles in Visible-Light Photocatalysis

Balázs Buchholcz,¹ Henrik Haspel,¹ Albert Oszkó,² Ákos Kukovecz^{1,3} and Zoltán Kónya^{1,4*}

¹Department of Applied and Environmental Chemistry, University of Szeged, H-6720 Szeged, Rerrich Béla tér 1, Hungary;

²Department of Physical Chemistry and Materials Science, University of Szeged, H-6720 Szeged, Rerrich Béla tér 1, Hungary;

³MTA-SZTE “Lendület” Porous Nanocomposites Research Group, H-6720 Szeged, Rerrich Béla tér 1, Hungary;

⁴MTA-SZTE Reaction Kinetics and Surface Chemistry Research Group, H-6720 Szeged, Rerrich Béla tér 1, Hungary;

Corresponding author: konya@chem.u-szeged.hu Tel.: +36-62-544-620

Supplementary Data

Table of Contents

Fig. S1: Nitrogen adsorption-desorption isotherms and the pores size distributions of the samples BNT1 and HTBNT1.

Table S1: BET surface areas and total pore volume of the nanostructures.

Fig. S2: XRD patterns of the BNT1 sample before and after thermal annealing.

Fig. S3: XRD patterns of the BNT1 and HTBNT1 samples.

Fig. S4: UV-VIS absorption spectra of the samples BNT1 and HTBNT1.

Fig. S5: UV-VIS absorption spectra of the pristine (a), the modified (BNT1 (c), BNT10 (e)) materials, and the samples calcined at 400 °C (HTNT (b), HTBNT1 (d), HTBNT10 (f)).

Fig. S6: Kubelka-Munk plots of the pristine, modified (BNT1, BNT10) and calcined (HTNT, HTBNT1, HTBNT10) titanate nanotubes.

Fig S7: Emission spectra of the mercury-vapor lamp with and without cut-off filter.

Fig. S8: UV-VIS spectra of the MO solutions before and after 1, 2, 4 and 8 h irradiation time for the NT, HTNT, BNT1, HTBNT1, BNT10, HTBNT10 and P25.

Fig S9: Photocatalytic degradation curves of MO by visible light irradiation.

Table S2. Photocatalytic properties of BiOX/TiOx photocatalysts in MO decolorization.

Fig S10: Band edge positions and the corresponding band gaps in BiOCl, TiONT and TiO₂.

Fig. S1 depicts the nitrogen adsorption-desorption isotherm and the corresponding pore size distribution of the BNT1 sample.

Fig S11: Basic characterization of bulk BiOCl. Panels (a) and (b) show SEM images of BiOCl, panel (c) depicts the UV-Vis absorption spectra and Tauc-plot (inset) and (d) is the comparison of XRD pattern of bulk BiOCl, NT, BNT10 and HTBNT10.

Fig S12: Photocatalytic degradation of MO (10 mg/L) using HTBNT10 catalyst (1.0 g/L) under visible light irradiation in five consecutive runs.

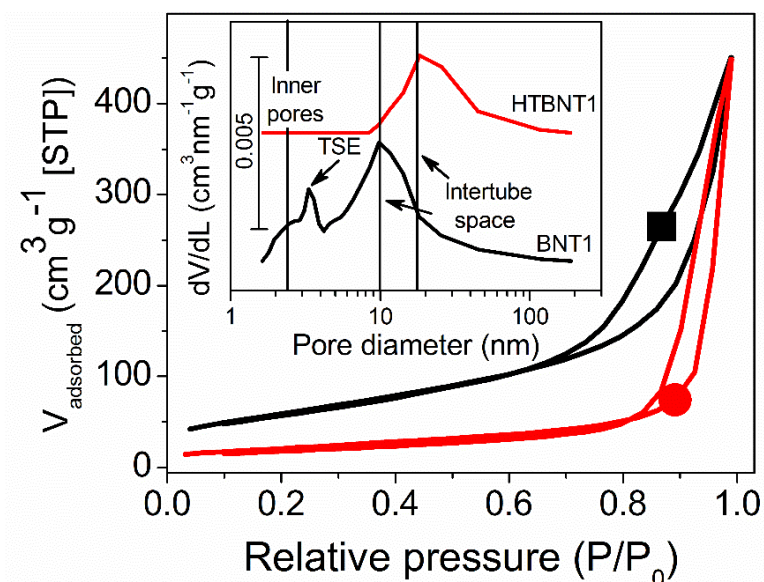


Fig. S1. Nitrogen adsorption-desorption isotherms and the corresponding pores size distributions (in inset graph) of the samples BNT1 (a) and HTBNT1 (b). The pore size distributions depicted in logarithmic scale. The “TSE” stands for the abbreviation of the “tensile strength effect” artifact.

Sample	a_s (m^2g^{-1})	V_{pore} (cm^3/g)
NT	224	0.70
BNT1	215	0.75
HTNT	106	0.64
HTBNT1	77	0.68

Table S1. BET surface areas and total pore volumes of the pristine and modified nanostructures.

Beside the pristine and 10% BiOCl decorated titanate nanotubes, we also annealed the 1% BiOCl sample at up to 900 °C for 1 h. The resulting phase transformation was monitored by XRD. Results are shown in Fig. S2.

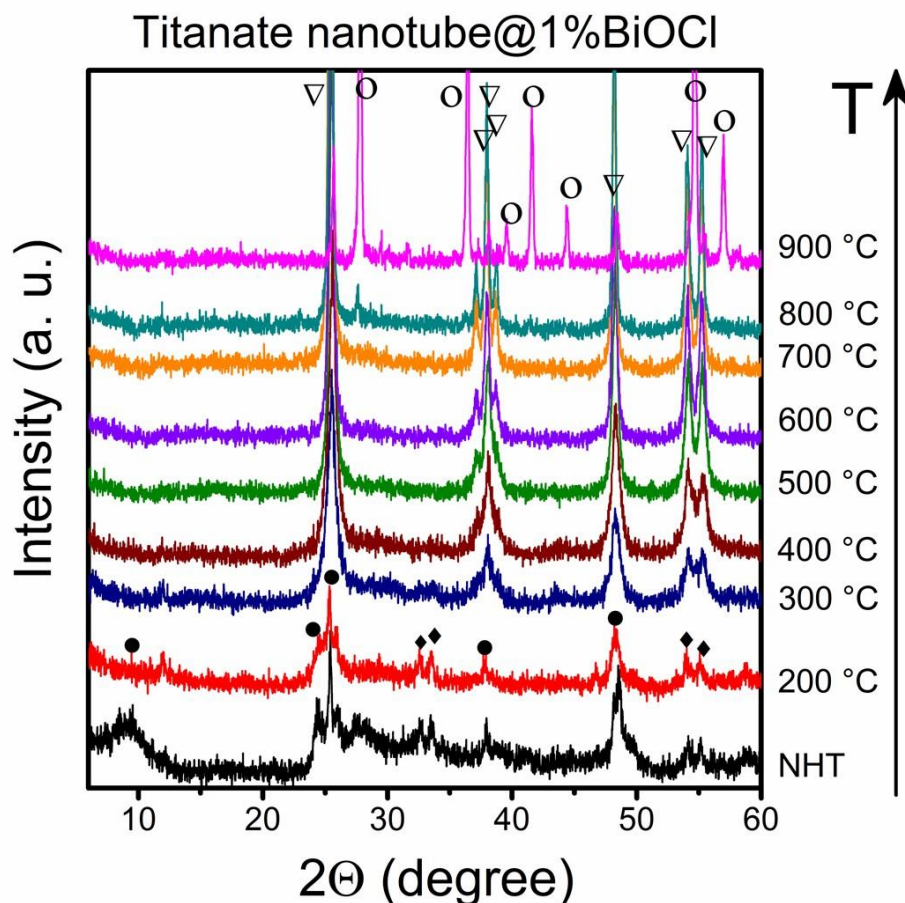


Fig. S2. XRD patterns of the BNT1 sample before and after thermal annealing. The symbol "●" belongs to trititanate, "∇" to anatase TiO₂, "○" to rutile TiO₂ and "◆" to BiOCl.

The XRD pattern of BNT1 shows similarities with that of the BNT10 sample, but the smaller BiOCl content allows the observation of both the trititanate and the BiOCl reflections. The formation of anatase phase is more dominant than in NT, but less dominant than in BNT10. Rutile TiO₂ phase starts to form at 800 °C. This finding further justifies our hypothesis, that increasing the BiOCl nanoparticle amount supports the anatase-rutile phase transformation.

Fig. S3 compares the XRD pattern of the BNT1 and BNT10 samples.

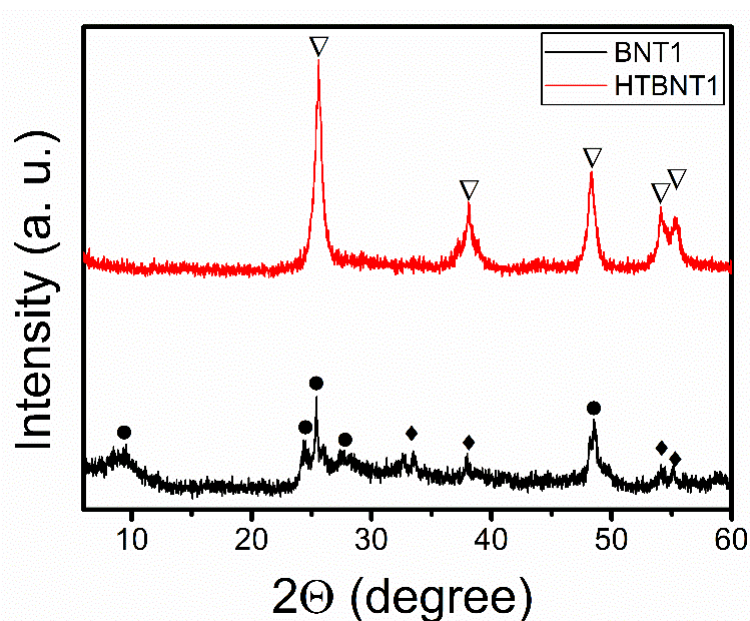


Fig. S3. XRD patterns of the BNT1 and HTBNT1 samples. The symbol “•” belongs to trititanate, “∇” to anatase TiO₂, and ♦ to BiOCl.

The BNT1 and the HTBNT1 XRD patterns are similar to those of BNT10 and HTBNT10. The as-formed anatase structure confirmed the titanate phase transformation.

Fig. S4 depicts the absorbance spectra of the BNT1 and HTBNT1 samples compared to that of P25. The steep region of P25 and the BNT1 is almost identical, but HTBNT1 spectra shifted to the higher wavelength, and thus to lower absorption energies.

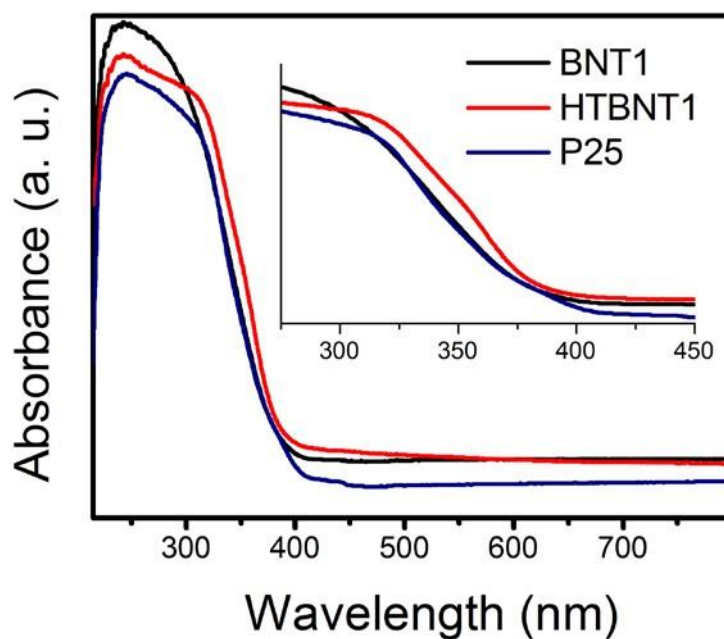


Fig. S4. UV-VIS absorption spectra of BNT1 and HTBNT1 compared to the that of P25.

Fig. S5 shows the the UV-VIS diffuse reflectance spectra in absorbance representation. E_g was estimated by the extrapolation of the steep range to the X-axis. We found a considerably lower band gap for HTBNT10 compared to the other samples.

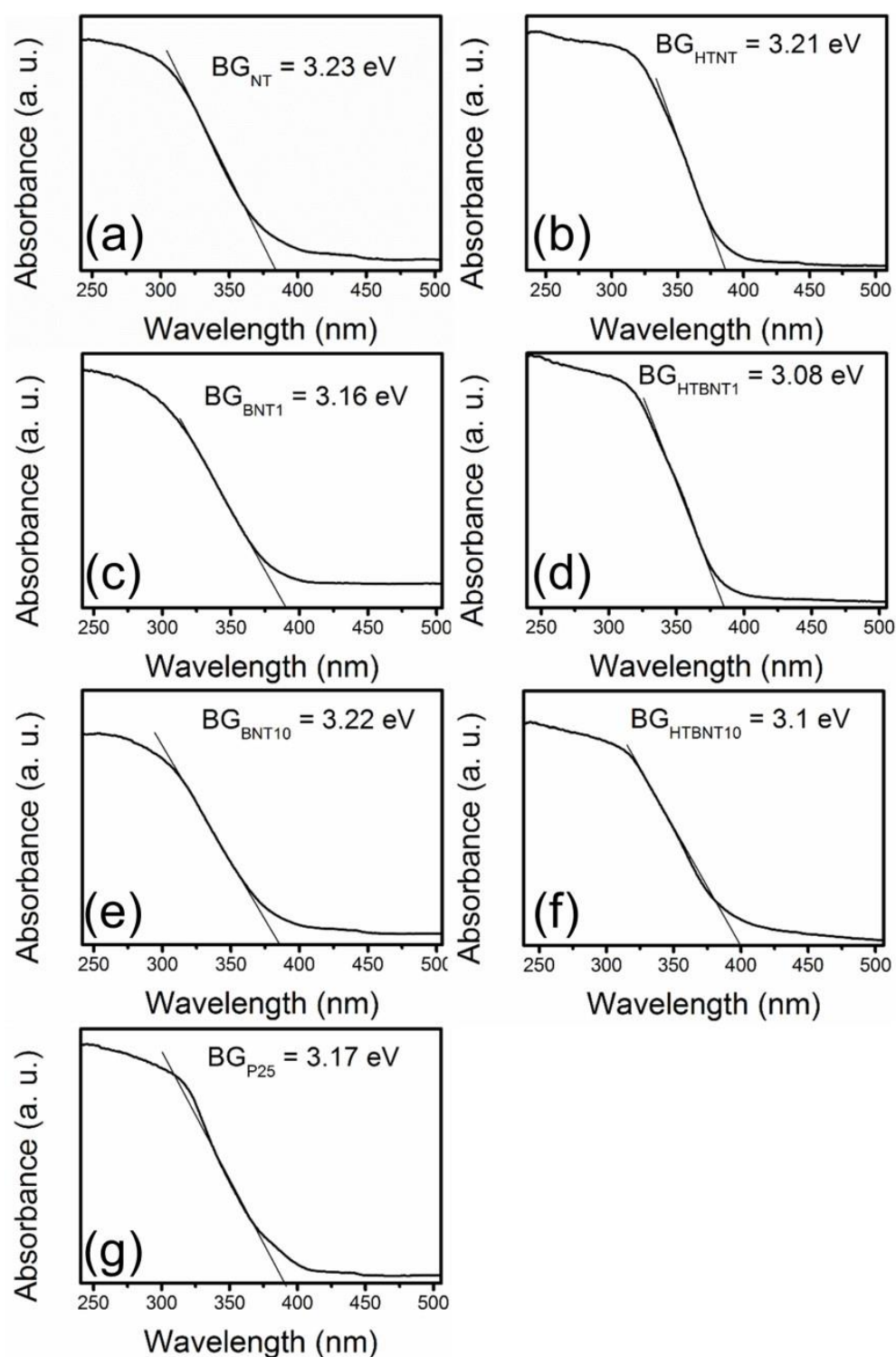


Fig. S5. UV-VIS absorption spectra of the pristine (a) and modified (BNT1 (c), BNT10 (e)) materials, and of the samples calcined at 400 °C (HTNT (b), HTBNT1 (d), HTBNT10 (f)). The result for P25 (g) was added for comparison.

Fig. S6 shows the UV-VIS diffuse reflectance spectra in the Kubelka-Munk representation. E_g was estimated by the extrapolation of the steep range to the X-axis. We found a considerably lower band gap for HTBNT10 compared to the other samples.

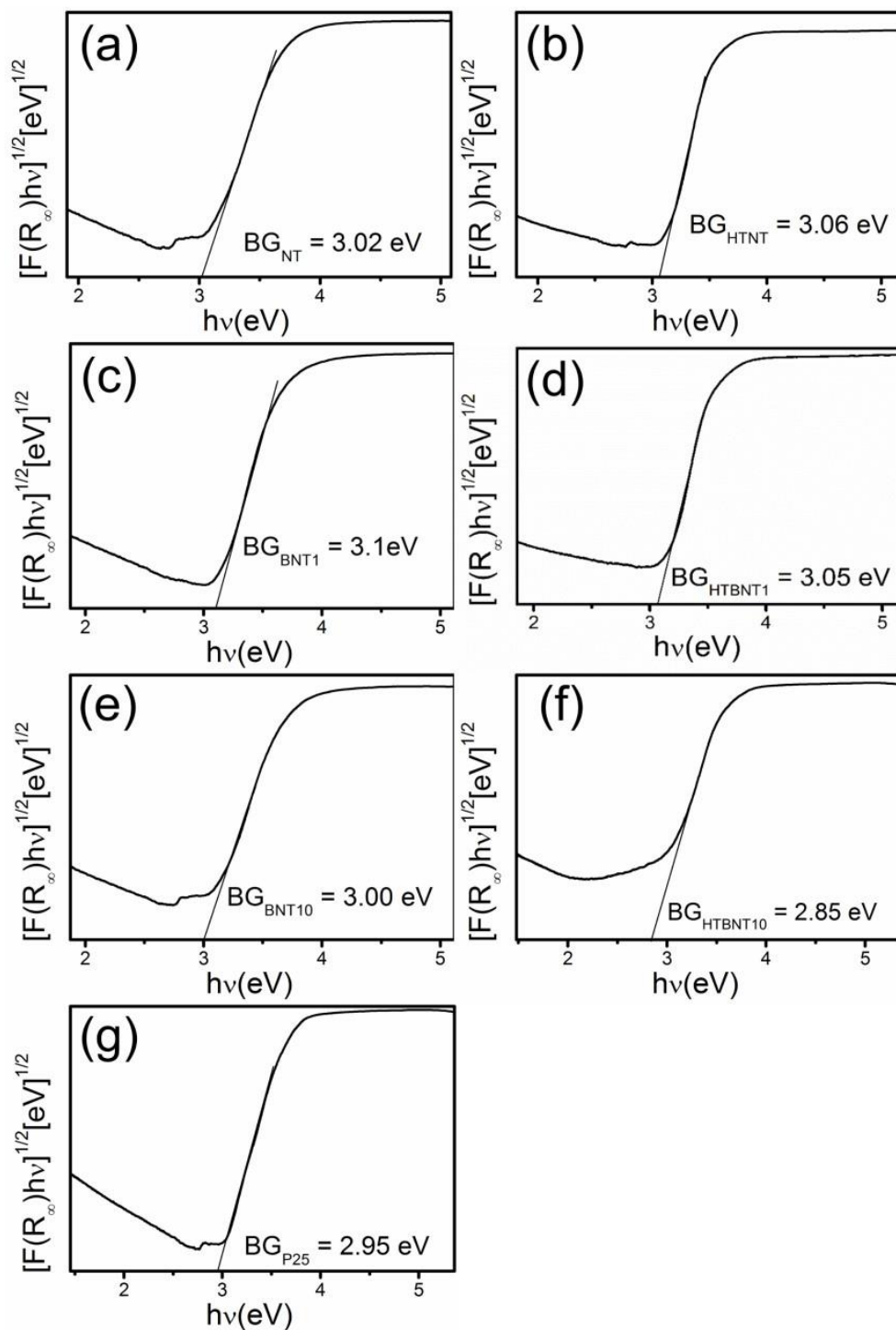


Fig. S6. UV-VIS absorption spectra of the pristine (a) and modified (BNT1 (c), BNT10 (e)), and of the samples calcined at 400 °C (HTNT (b), HTBNT1 (d), HTBNT10 (f)) in Kubelka Munk representation. Result for P25 (g) was added for comparison.

Fig. S7 shows the emission spectra of the used light source with and without UV filter

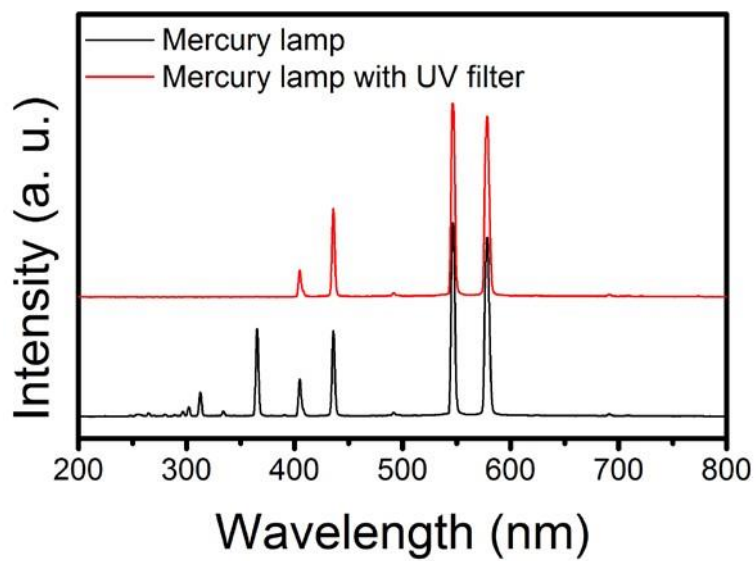


Fig. S7. Emission spectra of the applied mercury-vapor lamp with and without the used cut-off filter.

Fig. S8 depicts the UV-VIS spectra of MO before and after 1, 2, 4 and 8 hour visible light irradiation in the presence of NT (a), HTNT (b), BNT1 (c), HTBNT1 (d), BNT10 (e), HTBNT10 (f) and P25 (g)

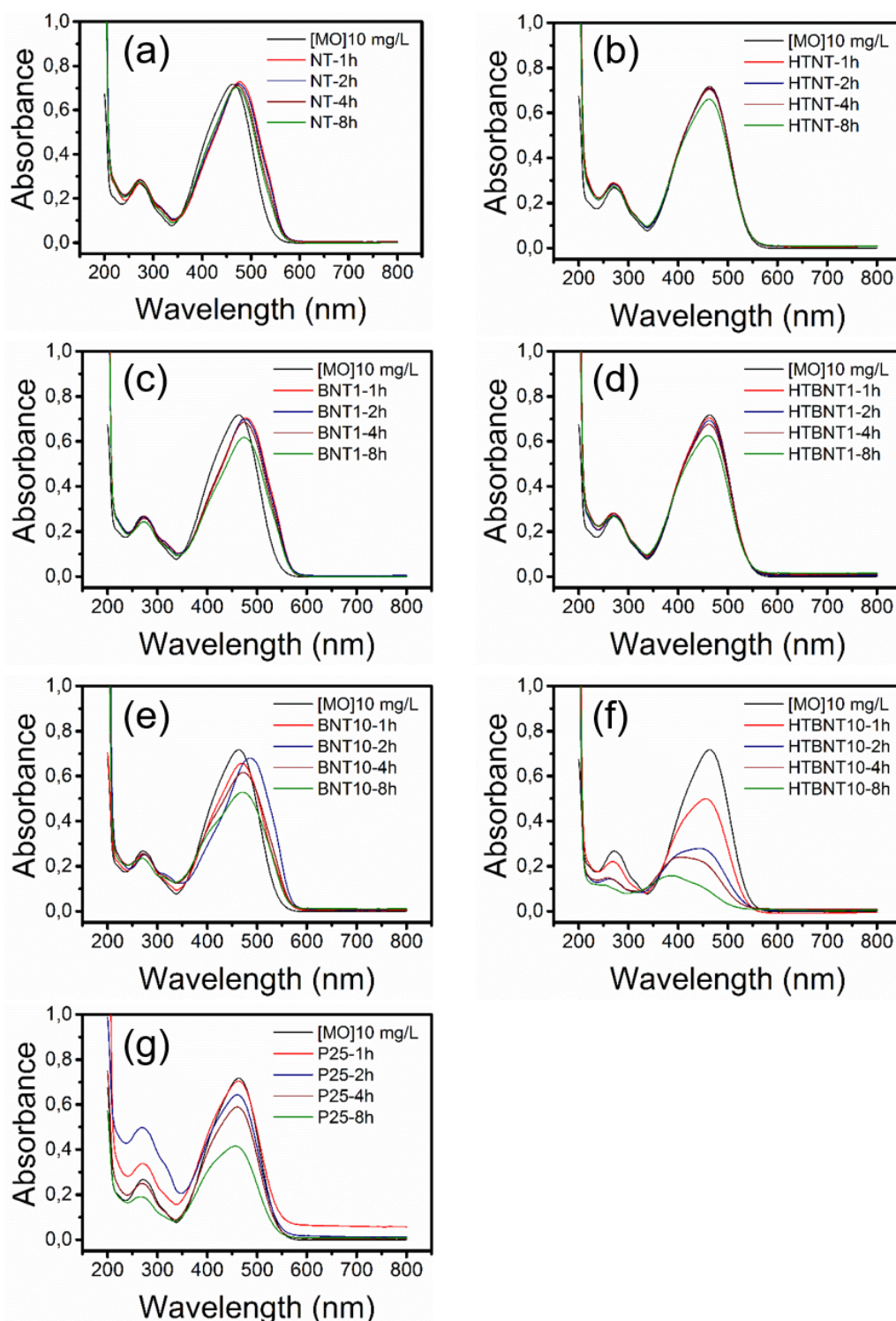


Fig. S8. UV-VIS spectra of the MO solutions before and after 1, 2, 4 and 8 h irradiation time for the catalyst NT (a), HTNT (b), BNT1 (c), HTBNT1 (d), BNT10 (e), HTBNT10 (f) and P25 (g).

Photocatalytic degradation curves (variation in MO concentration with irradiation time) (Fig. 9a), and the effect of photolysis and adsorption (Fig. 9b) in linear representation.

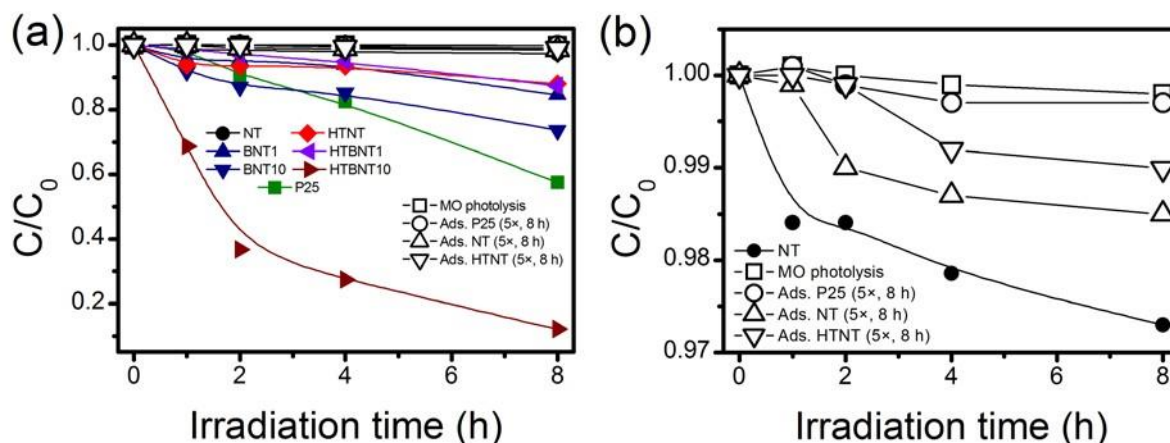


Fig. S9. Photocatalytic decolorization curves of methyl orange by visible light irradiation in linear ([MO] vs. irradiation time) representation for all investigated samples (NT, HTNT, BNT1, BNT10, HTBNT1 and HTBNT10) (a), and the effect of adsorption and photolysis on the decolorization of the organic dye (b).

Photocatalyst	Photocatalytic activity	Ref. photocatalyst	Enhancement	Ref.
BiOI/TiO ₂	95% (VIS) in 2 h	TiO ₂ (VIS): 1%	95	[1]
		BiOI (VIS): 2%	47	
BiOI/TiO ₂	57% (VIS) in 160 min	-	-	[2]
BiOCl/TiO ₂	84% (UVC) in 5 h	blank: 58%	1.5	[3]
	58% (UVA) in 5 h	blank: 1%	58	
BiOI/TiO ₂ /cotton	29% (VIS) in 1 h	cotton: 1%-	29	[4]
BiOCl/TiO ₂	64% (Sun) in 50 min		32	
BiOBr/TiO ₂	100% (Sun) in 50 min	blank: 2%-	50	[5]
BiOI/TiO ₂	52% (Sun) in 50 min		27	
BiOBr/TiO ₂ NTA	93% (VIS) in 3h	blank: 5%	23	[6]
BiOI/TiO ₂ NTA	67% (VIS) in 3 h	TiO ₂ NTA: 2%	33	[7]
BiOBr/TiO ₂	87% (VIS) in 80 min	a-TiO ₂ : 2%	43	[8]
BiOI/TiO ₂ NBA	97% (VIS) in 10 min	TiO ₂ NBA: 19%	5	[9]
		TiO ₂ : 2%	40	
BiOI/TiO ₂	80% (VIS) in 3h	BiOI: 9%	9	[10]
BiOI/TiO ₂	87% (VIS) in 2 h	blank: 1%	87	[11]
BiOI/TiO ₂	85% (UV-VIS) in 25 min	TiO ₂ : 51.5%	1.7	[12]

Table S2. Photocatalytic properties of BiOX/TiO_x photocatalysts in MO decolorization.

Fig. S10 summarizes literature data of the edge positions of the valence and conduction bands in BiOCl, TiONT, and TiO₂.

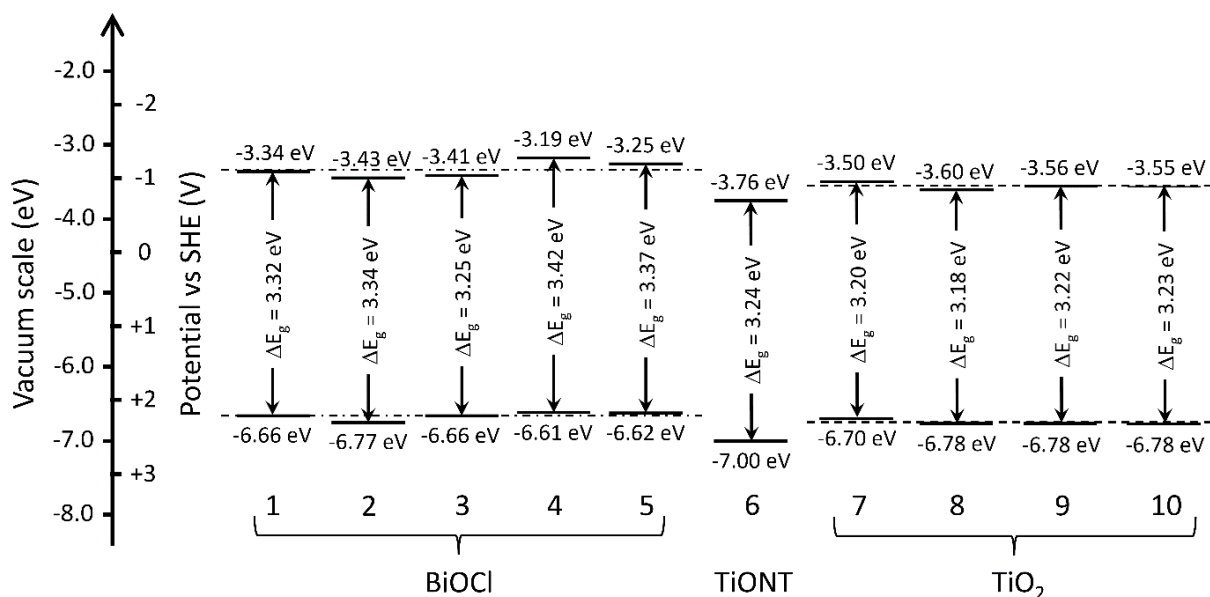


Fig. S10. Literature data on the band edge positions and the corresponding band gaps of BiOCl, TiONT and TiO₂. Values were taken from REF 1: App. Catal. B 158–159 (2014) 182-189, 2: Chem. Commun. 51 (2015) 2629-2632, 3: J. Am. Chem. Soc. 135 (2013) 10411, 4-5: ACS Catal. 5 (2015) 3540-3551, 6: Phys. Rev. B 75 (2007) 035423, 7: Nature Materials 12 (2013) 798, 8-9-10: Angew. Chem. Int. Ed. 123 (2011) 2181-2185.

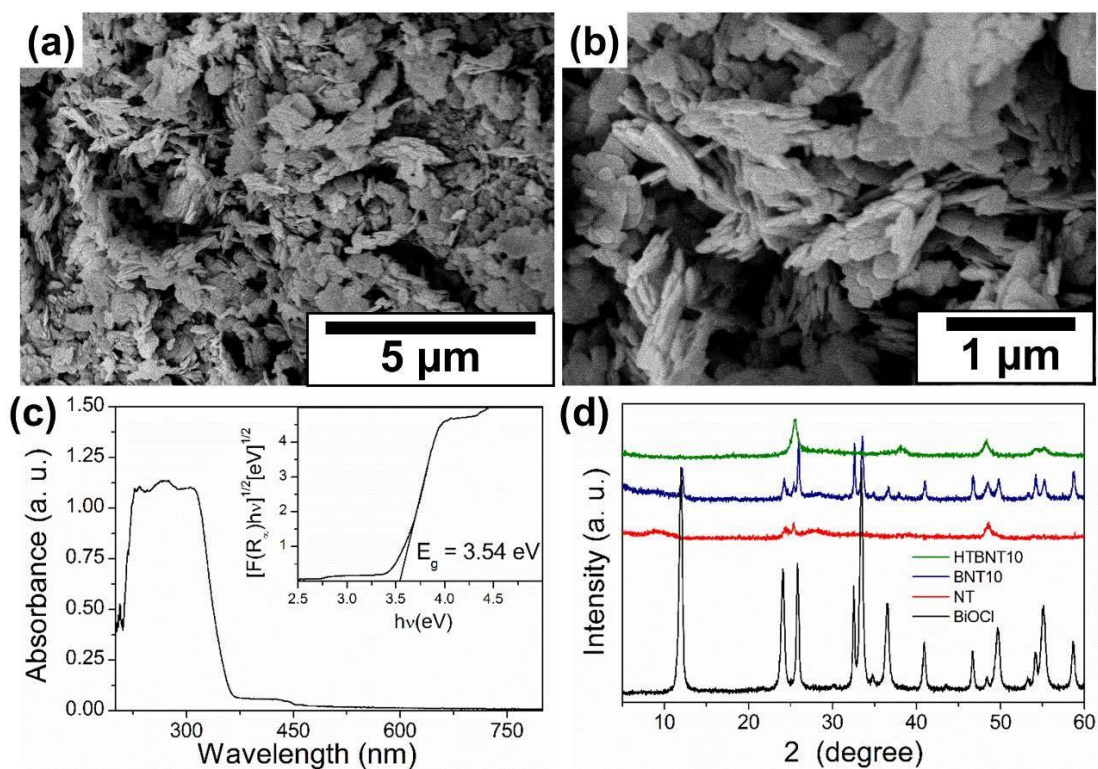


Fig S11: Basic characterization of bulk BiOCl. Panels (a) and (b) show SEM images of BiOCl, panel (c) depicts the UV-Vis absorption spectra and Tauc-plot (inset) and (d) is the comparison of XRD pattern of bulk BiOCl, NT, BNT10 and HTBNT10.

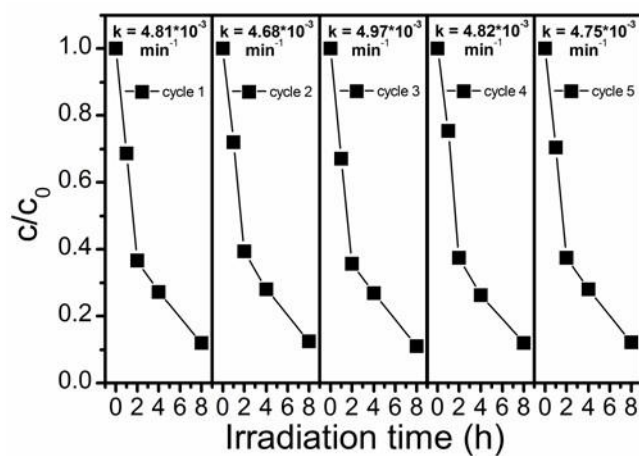


Fig S12: Photocatalytic degradation of MO (10 mg/L) using HTBNT10 catalyst (1.0 g/L) under visible light irradiation in five consecutive runs.

References

- [1] X. Zhang, L. Zhang, T. Xie, D. Wang, Low-Temperature Synthesis and High Visible-Light-Induced Photocatalytic Activity of BiOI/TiO₂ Heterostructures, *J. Phys. Chem. C* 113 (2009) 7371–7378.
- [2] G. Dai, J. Yu, G. Liu, Synthesis and Enhanced Visible-Light Photoelectrocatalytic Activity of p-n Junction BiOI/TiO₂ Nanotube Arrays, *J. Phys. Chem. C* 115 (2011) 7339-7346.
- [3] Y. Cai, P. Wang, Y. Ye, J. Liu, Z. Tian, Y. Liu, C. Liang, Grafting BiOCl nanosheets onto TiO₂ tubular arrays to form a hierarchical structure with improved photocatalytic performance, *RSC Adv.* 3 (2013) 19064-19069.
- [4] D. Wu, H. Wang, C. Li, J. Xia, X. Song, W. Huang, Photocatalytic self-cleaning properties of cotton fabrics functionalized with p-BiOI/n-TiO₂ heterojunction, *Surf. Coat. Tech.* 258 (2014) 672-676.
- [5] X. Cao, Z. Lu, L. Zhu, L. Yang, L. Gu, L. Cai, J. Chen, A new family of sunlight-driven bifunctional photocatalysts based on TiO₂ nanoribbon frameworks and bismuth oxohalide nanoplates, *Nanoscale* 6 (2014) 1434-1444.
- [6] L. Ruan, J. Liu, Q. Zhou, J. Hu, G. Xu, X. Shu, Y. Wu, A flake-tube structured BiOBr–TiO₂ nanotube array heterojunction with enhanced visible light photocatalytic activity, *New J. Chem.* 38 (2014) 3022-3028.
- [7] J. Liu, L. Ruan, S. B. Adelojuc, Y. Wu, BiOI/TiO₂ nanotube arrays, a unique flake-tube structured p–n junction with remarkable visible-light photoelectrocatalytic performance and stability, *Dalton Trans.* 43 (2014) 1706-1715.
- [8] X. Wang, W. Yang, F. Li, J. Zhao, R. Liu, S. Liu, B. Li, Construction of amorphous TiO₂/BiOBr heterojunctions via facets coupling for enhanced photocatalytic activity, *J. Hazard. Mater.* 292 (2015) 126-136.
- [9] Q. Teng, X. Zhou, B. Jin, J. Luo, X. Xu, H. Guan, W. Wang, F. Yang, Synthesis and enhanced photocatalytic activity of a BiOI/TiO₂ nanobelt array for methyl orange degradation under visible light irradiation, *RSC Adv.* 6 (2016) 36881-36887.
- [10] Z. Liu, X. Xu, J. Fang, X. Zhu, J. Chu, B. Li, Microemulsion synthesis, characterization of bismuth oxyiodine/titanium dioxide hybrid nanoparticles with outstanding photocatalytic performance under visible light irradiation, *Appl. Surface Sci.* 258 (2012) 3771-3778.
- [11] Z. Li, M. Wang, J. Shen, Z. Zhu, Y. Liu, Synthesis of BiOI nanosheet/coarsened TiO₂ nanobelt heterostructures for enhancing visible light photocatalytic activity, *RSC Adv.* 6 (2016) 30037-30047.

[12] J. Li, J. Zhong, Y. Si, S. Huang, L. Dou, M. Li, Y. Liu, J. Ding, Improved solar-driven photocatalytic performance of BiOI decorated TiO₂ benefiting from the separation properties of photo-induced charge carriers, *Solid State Sciences* 52 (2016) 106-111.